Implementation and Validation of Non-Drag Interfacial Forces in CFX-5.6

Jun-Mei Shi[1], Thomas Frank[2], Eckhard Krepper[1], Dirk Lucas[1], Ulrich Rohde[1] and Horst-Michael Prasser[1]

1: Institute for Safety Research, FZR, Bautzner Landstrasse 128, 01328 Dresden, Germany,
J.Shi@fz–rossendorf.de
2: ANSYS Germany, Staudenfeldweg 12, 83624 Otterfing, Germany,
Thomas.Frank@ansys.com

Abstract In Eulerian-Eulerian modeling of multiphase flow, closure models are needed for interfacial forces. The present work was concentrated on the non-drag forces, namely the lift, virtual mass, turbulent dispersion and wall lubrication force. They are reported to be mainly responsible for the gas volume fraction distribution in a vertical bubbly flow. Different models were proposed in the literature for each of these forces. In this work, we implemented a number of non-drag force models in the Eulerian multiphase flow package of the commercial code CFX-5.6 in order to enhance its application range. Extensive numerical experiments were carried out in order to examine their numerical properties (convergence characteristics, grid dependence of the results) and to evaluate their validity. The evaluation was based on the experimental database for upward air-water flows in a vertical pipe established at Forschungszentrum Rossendorf (FZR) using the fast wiremesh sensor measurement technique. In all simulations a zero-equation model was used for the dispersed phase whereas two different turbulence models, namely the k-ε and SST model, were investigated for the liquid phase. The bubble induced turbulence was taken into account by the Sato model. Fairly good agreements were observed between the numerical solutions and measurements for all test cases when the SST model was chosen together with the Tomiyama correlations for the lift and wall lubrication force and the Favré-Averaged Drag (FAD) model for the turbulent dispersion force due to Burns (2001). The results clearly show the advantage of the FAD model over the widely applied model by Lopez de Bertodano et al. (1994). In addition, the investigation also indicates that further efforts in multiphase phase flow turbulence modeling and in near-wall treatment are very necessary.

1 Introduction

In Eulerian modeling of multiphase flow, the continuum model equations are usually derived based on various average approaches (see, e.g., Ishii, 1975; Drew and Passman, 1999; Simonin, 2000). Information of interfacial boundary and interfacial transport is lost for the continuum modeling and hence additional closure models are needed for them. The predictability of an Eulerian code strongly depends on the quality of the interfacial closure models. Until now, interfacial transport modeling in gas-liquid flows including interfacial forces still have to mainly rely on empirical methods due to the complexity of the problem. Together with coalescence and breakup and multiphase turbulence, modeling of the interfacial forces and other interfacial transport processes remain as the main challenge in CFD development for gas-liquid flows.

The present study was focused on the closure laws for non-drag interfacial forces including lift, turbulent dispersion and wall force in bubbly flows. These forces have received increasing attention in recent years since they have a crucial influence on the lateral motion of bubbles in vertical gas-liquid flows (Tomiyama, 1998). Compared with the drag force, non-drag forces have a much more complicated nature. Experimental studies have revealed that the bubble size has a strong effect on the distribution of gas volume fraction, namely a wall peak is observed for bubbles with a diameter smaller than 6 mm in contrast to a core peak for larger bubbles in an air-water flow (Liu, 1993; Prasser et al., 2001, 2002). This is mainly due to the deformation

for larger bubbles, which causes the lift force to change sign. A number of mechanisms are now identified that can induce a transverse lift force on a rising bubble, e.g., shear, bubble deformation or asymmetrical bubble wake (Magnaudet and Eames, 2000; Tomiyama et al., 1999). Due to this fact, there exist different empirical correlations for the lift force in the literature, which differ from each other in parameter dependence, magnitude and range of validity (Frank, 2002, 2003). Moreover, due to the difficulties in theoretical modeling and measurements, some models, e.g., the wall lubrication force model by Antal et al. (1991), were more like being proposed rather than being derived because of the oversimplification or unphysical assumption introduced in their derivation. Their model constants have to be calibrated for each application. Recently, significant progress is seen in modeling of the turbulent dispersion force by considering the turbulence effect on the drag force (Lopez de Bertodano, 1998; Drew, 2001; Moraga et al., 2003; Burns et al., 2004). Advances were also reported in improving the lift and the wall lubrication force models (see, e.g., Legendre and Magnaudet, 1998; Tomiyama, 1998; Tomiyama et al., 1999).

Good non-drag force models are essential for correct prediction of gas volume fraction distribution in a number of industrial applications. Despite the progress mentioned above, the available correlations still contain a lot of uncertainties. Closure models have to be validated and model constants have to be carefully calibrated for a wide range of applications. In this work, we implemented a number of non-drag force correlations available in the literature in the Eulerian multiphase flow package of the commercial code CFX-5.6. Extensive numerical experiments were carried out in order to examine their validity and grid convergence characteristics. The evaluation was based on the experimental database of upward air-water bubbly flow in a vertical pipe measured at the FZR MT-Loop facility using the fast wire-mesh sensor (Prasser et al., 2003; Lucas et al., 2003), which was established for the purpose of multiphase CFD code validation and model development. In addition, the effect of the liquid phase turbulence models was also examined.

2 Governing equations

In this study, we consider the isothermal bubbly flow without interfacial mass transfer and assume both fluids to be incompressible. Adopting the eddy viscosity hypothesis, the Reynolds averaged governing equations for mass and momentum transport of CFX-5.6 two-fluid model can be written as follows:

$$\frac{\partial}{\partial t}(\alpha_k \rho_k) + \nabla \cdot (\alpha_k \rho_k \mathbf{U}_k) = 0 \tag{1}$$

$$\frac{\partial}{\partial t}(\alpha_k \rho_k \mathbf{U}_k) + \nabla \cdot (\alpha_k \rho_k \mathbf{U}_k \mathbf{U}_k) = -\alpha_k \nabla P - \nabla \cdot \left[\alpha_k \mu_{k,eff} \left(\nabla \mathbf{U}_k + \nabla^{\mathbf{T}} \mathbf{U}_k\right)\right] + \alpha_k \rho_k \mathbf{g}_k + \mathbf{M}_k \tag{2}$$

where k is the phase indicator, namely $k = \ell$ representing the liquid and $k = g$ the gas phase, α the volume fraction, $\mathbf{U}$ the velocity, P the pressure shared by both phases, $\mu_{k,eff}$ the effective dynamic viscosity consisting of the material (μ_k) and turbulence eddy ($\mu_{k,t}$) contributions, $\mathbf{g}$ the gravity acceleration, and $\mathbf{M}$ the interfacial forces including the drag ($\mathbf{F_D}$), lift ($\mathbf{F_L}$), wall lubrication ($\mathbf{F_W}$) and turbulence dispersion force ($\mathbf{F_{TD}}$). All these quantities are Reynolds averaged except for $\mathbf{U}$, which takes the Favré averaged value (mass-weighted average). Some higher order correlations resulting from Reynolds averaging were neglected. In addition, the added mass force was neglected in the present study due to the restriction to the steady state investigation.

Two turbulence models, the standard k-ε and the Shear-Stress-Transport (SST) model by Menter (1994), were applied to the liquid phase turbulence. The gas phase turbulence was approximated by a zero equation model, which assumes a gas turbulent eddy viscosity to be proportional to that of the liquid phase. The bubble induced turbulence was taken into account following the model by Sato et al. (1981), which adds a bubble induced eddy viscosity to the fluid phase turbulence. The Grace model was chosen for the drag force. The closure models for the non-drag forces are described separately.

3 Non-drag force closure models

In order to extend the application range of the Eulerian multiphase flow package of the commercial code CFX-5.6, we implemented a number of non-drag force models available in the literature as CFX USER Fortran Routines and or simply by CFX Command Language (CCL). The implementation was mainly based on a literature review by Frank (2002, 2003) and also included closure models for solid particles and droplets.

3.1 Lift force

The lift force plays a deciding role in determining the gas volume fraction distribution in a vertical bubbly flow. Considering this situation, we implemented the following lift force models into CFX-5.6, including the analytical solution by Saffman (1965b,a) for a sphere at low Reynolds number and small linear shear limit, the extension to finite Reynolds numbers (correlation) for solid particle (Mei, 1992) and for spherical bubble (Mei and Clausner, 1994), a correlation by Legendre and Magnaudet (1998) for bubbles, a correlation of Moraga et al. (1999) for high Reynolds number solid particles, and the Tomiyama correlation for deformable bubbles (Tomiyama, 1998). As mentioned above, different lift force formulations were applied in the literature. In this paper we adopt the definition proposed by Auton (1987), i.e.

$$\mathbf{F}_\mathbf{L}^g = -C_L \alpha_g \rho_\ell (\mathbf{U}_g - \mathbf{U}_\ell) \times \nabla \times \mathbf{U}_\ell \tag{3}$$

where C_L is the lift coefficient. Correlations using other definitions were converted into eq. (3).

In the present study, deformable bubbles with a diameter d_p between 3 to 5 mm and a bubble Reynolds number from several hundreds to thousand were encountered. Hence the Tomiyama correlation is the most suitable choice. Based on a series of numerical and experimental investigations, Tomiyama and coworkers were able to confirm that lift force on a bubble not only depends on the bubble Reynolds number, $Re_p = |\mathbf{U}_g - \mathbf{U}_\ell|\, d_p/\nu_\ell$, but also on the Eötvös number (Tomiyama et al., 1995; Tomiyama, 1998). Their model, after replacing -0.29 by -0.27 for continuous consideration, reads

$$C_L = \begin{cases} \min[0.288 \tanh(0.121 Re_p), f(Eo_d)], & Eo_d < 4 \\ f(Eo_d) = 0.00105 Eo_d^3 - 0.0159 Eo_d^2 - 0.0204 Eo_d + 0.474, & 4 \le Eo_d \le 10 \\ -0.27, & Eo_d > 10 \end{cases} \tag{4}$$

where Eo_d is the Eötvös number based on the long axis d_H of a deformable bubble, i.e.

$$Eo_d = \frac{(\rho_\ell - \rho_g)\, g_{eff}\, d_H^2}{\sigma^2}, \text{ with } d_H = d_p(1 + 0.163 Eo^{0.757})^{1/3} \text{ and } Eo = \frac{(\rho_\ell - \rho_g)\, g_{eff}\, d_p^2}{\sigma^2} \tag{5}$$

Equation (4) indicates that the lift coefficient decreases from positive to negative values (lift force pointing to the side of higher relative velocity) with increasing bubble diameter. This is caused by deformation and asymmetrical wake occurring with large bubbles (Tomiyama et al.,

1995). For air-water system under atmospheric pressure and the ambient temperature, the sign change occurs at a critical diameter,$d_p \approx 5.8$ mm according to eq. (4). It is generally believed that a positive lift force is responsible for the wall gas peak observed for vertical bubbly flows with small bubble diameters whereas a core gas peak is caused by a negative lift force occurring for large bubbles. In addition, negative lift coefficient was also reported for solid particles at large Re_p Reynold numbers from empirical investigation (Moraga et al., 1999) or for Re_p based on numerical simulation (Kurose et al., 2001).

3.2 Wall lubrication force

Moving bubbles in a near-wall flow region will receive a repulsive force from the wall due to the pressure difference over the bubble surface. This force might be similar to the force occuring in the fluid lubrication (viscous flow) and hence is sometimes refereed to as the wall lubrication force in literature. A model due to Antal et al. (1991), which is derived from the potential theory, is available in CFX-5.6, i.e.

$$\mathbf{F}^g_{\mathbf{W}} = -\alpha_g \rho_\ell |\mathbf{U_r} - (\mathbf{U_r} \cdot \mathbf{n_w})\mathbf{n_w}|^2 \max\left(C_1 + C_2 \frac{d_p}{y_w}, 0\right) \mathbf{n_w} \tag{6}$$

where $\mathbf{U_r} = \mathbf{U}_g - \mathbf{U}_\ell$ is the slip velocity between two phases and y_w the distance to wall. The model coefficient has to be calibrated for each application. CFX5 recommends $C_1 = -0.01$, $C_2 = 0.05$ while Krepper and Prasser (2000) obtained $C_1 = -0.0064$, $C_2 = 0.05$ by fitting their numerical results to the same experimental database as used for the present study.

In this work, another model applied by Tomiyama (1998) in their vertical pipe flow simulations was implemented, which is

$$\mathbf{F}^g_{\mathbf{W}} = -C_W \alpha_g \rho_\ell |\mathbf{U_r} - (\mathbf{U_r} \cdot \mathbf{n_w})\mathbf{n_w}|^2 \frac{d_p}{2} \left[\frac{1}{y_w^2} - \frac{1}{(D - y_w)^2}\right] \mathbf{n_w} \tag{7}$$

with a coefficient as a function of the Eötvös number,

$$C_W = \begin{cases} \exp(-0.933Eo + 0.179) & \text{if } 1 \le Eo \le 5, \\ \min(0.0059905Eo - 0.0186865, 0.179) & \text{if } Eo > 5 \end{cases} \tag{8}$$

Comparisons were carried out for both models in this study.

3.3 Turbulent dispersion force

In the Eulerian model, turbulent dispersion force can be estimated from the correlation of the first moments of the interfacial forces. A model proposed by Lopez de Bertodano et al. (1994) is implemented in CFX-5.6,

$$\mathbf{F}^g_{\mathbf{TD}} = -C_{TD} \rho_\ell k_\ell \nabla \alpha_g \tag{9}$$

which is proportional to the fluid turbulence kinetic energy and the gradient of the gas volume fraction. A constant coefficient, C_{TD} between 0.1 and 0.5 was recommended in CFX5 user documentation. Here we refer to it as RPI model for its origin of the place (Rensselaer Polytechnic Institute).

Recently, several authors (Lopez de Bertodano, 1998; Drew, 2001; Burns, 2001; Burns et al., 2004) have developed rigorous mathematical model derivation by considering the turbulence effect on the drag force from different approaches. We implemented the model by Burns (2001), refered to as the FAD model (Burns et al., 2004), in CFX-5.6. This model adopts the Favré averaged velocity and thus avoids a diffusion term in the continuity equation. Considering a

two-phase flow and applying Reynolds averaging to the drag force on the dispersed phase with a diameter d_p leads to a mean drag and a turbulent dispersion force term as follows,

$$\mathbf{F}^g_{\mathbf{TD}} = -\frac{3}{4}\alpha_g\,\rho_\ell\,\frac{C_D|U_r|}{d_p}\left(\frac{\overline{\alpha'_\ell \mathbf{u}'_\ell}}{\alpha_\ell} - \frac{\overline{\alpha'_g \mathbf{u}'_\ell}}{\alpha_g}\right) \tag{10}$$

In a two fluid model as considered in the present study, eq. (10) can be reformulated in analogy to the RPI model by adopting the eddy diffusity hypothesis. The result is equivalent to using a functional coefficient in eq. (9) , i.e.

$$C_{TD} = \frac{3}{4}\frac{C_D|U_r|\nu_{t,\ell}}{\sigma_g d_p k_\ell}\frac{1}{1-\alpha_g}. \tag{11}$$

where C_D is the drag coefficient, $|U_r| = |\mathbf{U}_g - \mathbf{U}_\ell|$ the relative velocity, $\nu_{t,\ell}$ the eddy viscosity and σ_g the turbulence Prandtl number for the volume fraction dispersion, which is estimated to be of order unity .Here we simply assumed $\sigma_g = 1$ in this study.

It is worth mentioning that Gosman et al. (1992) might be the first to adopt the Favré averaged velocity for multiphase flow turbulence modeling. Nevertheless, the turbulent dispersion force term in their model differs slightly from the Burn's model, namely $\frac{1}{1-\alpha_g}$ in eq. (11) to be replaced by $\frac{1}{(1-\alpha_g)^2}$ under the same assumptions adopted above. In addition, according to a detailed discusion in Moraga et al. (2003), the models by Lopez de Bertodano (1998) and Drew (2001) are equivalent to each other at small Stokes numbers ($St = \tau_d/\tau_e$), namely both corresponding to taking $C_{TD} = C_\mu^{1/4}/St$ with $C_\mu = 0.09$. The bubble response time can be estimated as $\tau_d = \frac{4}{3}\frac{d_p}{C_D\,|U_r|}$ and the eddy life time τ_e=$C_\mu^{3/4}\frac{k_\ell}{\varepsilon_\ell}$ using the k-ε model. Then considering $\nu_{t,\ell} = C_\mu\,k_\ell/\varepsilon_\ell$, their models lead to

$$C_{TD} = \frac{3}{4}\frac{C_D|U_r|\nu_{t,\ell}}{d_p k_\ell}. \tag{12}$$

which only differs from eq. (11) by a factor $\frac{1}{\sigma_g\,(1-\alpha_g)}$. These small differences among various models were not expected to have significant consequence on the numerical results in the present study where $\alpha_g < 10\%$. Hence it is already representative only to compare the FAD and RPI model.

4 Test case definitions

Extensive experimental data of gas volume fraction distributions in upward vertical air-water pipe flows have been obtained at FZR using the fast wiremesh sensor (Prasser et al., 1998, 2001, 2002). The database was established for the purpose of multiphase CFD code validation and model development. The assessment of the non-drag force models was based on the measurements at the MT-Loop test facility (Prasser et al., 2003). The test section is 4 m long and has an inner diameter of 51.2 mm. Air was injected into the upward water flow using a sparger consisting of 19 capilaries equally distributed over the cross section of the pipe in order to ensure axi-symmetry of the macroscopic flow. Measurements were carried out for stationary flows covering a wide range of air-water superficial velocity ratios at 10 different cross sections located between $L/D = 0.6$ and 59.2 from the gas injection using a wiremesh sensor with 24×24 electrodes. Details about the experimental set up and data accuracy are provided in (Lucas et al., 2002; Prasser et al., 2003). Test cases were defined within the bubbly flow regime with wall gas peaks, which is the most suitable for evaluating the turbulent dispersion force model.

The validation was based on the measurement data at the cross section $L/D = 59.2$ where the uncertainties due to the inlet conditions is expected to be the smallest. A list of the test cases together with the inlet superficial velocities of both phases corresponding to the atmospheric pressure and the ambient temperature and the mean bubble diameter measured at $L/D = 59.2$, which were needed as input parameters for the numerical simulation, is given in Table 1.

Test case	$U_{\ell,sup}$ [m/s]	$U_{g,sup}$ [m/s]	mean d_p [mm]
017	0.405	0.0040	4.8
019	1.017	0.0040	4.8
038	0.225	0.0096	4.3
039	0.405	0.0096	4.5
040	0.641	0.0096	4.6
041	1.017	0.0096	4.5
042	1.611	0.0096	3.6
074	1.017	0.0368	4.5

Table 1: Test case definition.

5 Validation and evaluation

5.1 Numerical settings

Considering the axial-symmetry of the flow, pseudo-2D simulations were carried out on a computational domain consisting of a 3 degree sector of the pipe. The symmetry condition was applied on both sector faces. A no-slip condition together with the CFX5 build-in wall functions for the turbulence models was applied for the liquid at the wall, whereas a free-slip wall condition was assumed for the gas. It is worth mentioning that the inlet superficial velocities provided in Table 1 were not sufficient for the definition of the inlet boundary condition in a three-dimentional simulation. Therefore, assumptions had to be introduced for inlet distributions. A uniform gas and liquid volume fraction profile in combination with various axial velocity profiles (U_{in}) and a medium turbulence intensity (5%) was assigned there. The radial velocity was assumed to be zero. As will be discussed in detail in section 5.2, the inlet profile was found to have no effect on the gas volume fraction distribution at $L/D = 59.2$. The outlet was located at 3.3 m away from the inlet, where an averaged static pressure equal to the atmospheric pressure P_0 was assigned. Both fluids were assumed to be incompressible and the bubble diameter was assumed to be constant within the total computational domain. A suitable pressure initialization was found to be essential for the convergence since a large buoyancy force was acting on the gas phase due to the high density ratio between water and air. The pressure field was initialized using the expression $P = P_0 + \rho_\ell |\mathbf{g}|(3.3 - L)$.

In order to examine the grid convergence of the numerical results, five computational grids with different local grid resolutions were applied (Table 2). The grid size was increasingly reduced from the pipe center ($\triangle y_1$) towards the wall ($\triangle y_n$) as indicated by their ratio $\triangle y_1/\triangle y_n$. The maximum values of the near-wall resolution in wall units of case FZR-074 were also provided in Table 2 for reference.

As will be discussed in the following paragraph, the SST model in combination with the FAD model for the turbulent dispersion force and the Tomiyama lift (4) and wall lubrication force model (7) produces best agreements with measurement data. If no other explicit specification is given, these models are implied.

grid	$\triangle y_1/\triangle y_n$	y^+_{max} (FZR-074)	grid	$\triangle y_1/\triangle y_n$	y^+_{max} (FZR-074)
y25x400	5	26.8	y35x600b	10	12.6
y35x600a	5	19.5	y35x600c	2.5	29.1
y50x800	5	13.9			

Table 2: Computational grids, $y n x m$ means n grid points in the radial direction and m in the axial direction.

5.2 Examination of convergence criteria, grid dependence and inlet effect

The total gas volume fraction in the computational domain is expected to reach a constant value when a stationary flow computation converges. Hence the gas holdup (the volume average) in the total domain was used as an additional convergence indicator. This measure is useful for calculations over a computational domain with an especially large aspect ratio as considered in the present study. It was found that the RMS (root mean square) residual of the continuity equations have to be reduced to a magnitude of 10^{-4} so that the gas holdup approaches to the final value. This conclusion was found to apply to all grids. As an example, the evolution of the gas holdup vs. the RMS residual of the air volume fraction equation is demonstrated for the case FZR-042 in Fig. 1. In order to ensure a small iteration error in the numerical solution, convergence was accepted when the RMS residual of all governing equations was decreased below 10^{-5}. This criteria is expected to be safe.

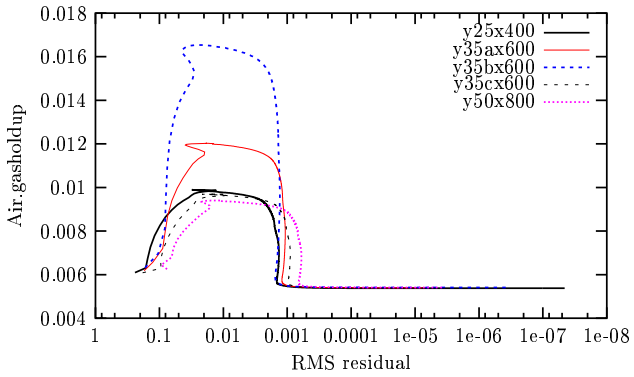

Figure 1: FZR-042: gas holdup vs. RMS residual for various grids.

Then, the grid dependence of the numerical results was examined. As an example, the volume fraction profile and the radial distribution of the non-drag forces at $L/D = 59.2$ obtained using various grids are displayed in Fig. 2 for case FZR-042. The results almost coincide with each other except for the peak regions. In these regions, the grid resolution of $y35x600c$ and $y25x400$ was not sufficient, whereas the other grids, $y50x800$, $y35x600a$ and $y35x600b$, produced smooth solutions close to each other. Hence grid-independent numerical solutions can be obtained with the latter three grids. 3D simulations were also carried out using a 60 degree sector of the pipe (Frank et al., 2004), which confirmed the present pseudo 2D results.

In order to further reduce uncertainty that might be introduced by the assumption adopted for the inlet condition, numerical experiments were performed by using various inlet velocity profiles or gas volume fraction distributions keeping at the same time the superficial velocities unchanged. The profile shape is defined as follows, uniform, $\phi_{in} = \phi_0$, parabolic, $\phi_{in} = 2\phi_0\,(1 - r^{*2})$, 1/6-th power, $\phi_{in} = 1.264\phi_0\,(1-r^*)^{1/6}$, and 1/7-th power, $\phi_{in} = 1.224\phi_0\,(1-r^*)^{1/7}$, where ϕ_0 is the mean value and $r^* = 2r/D$ the dimensionless radial coordinate. The results for the

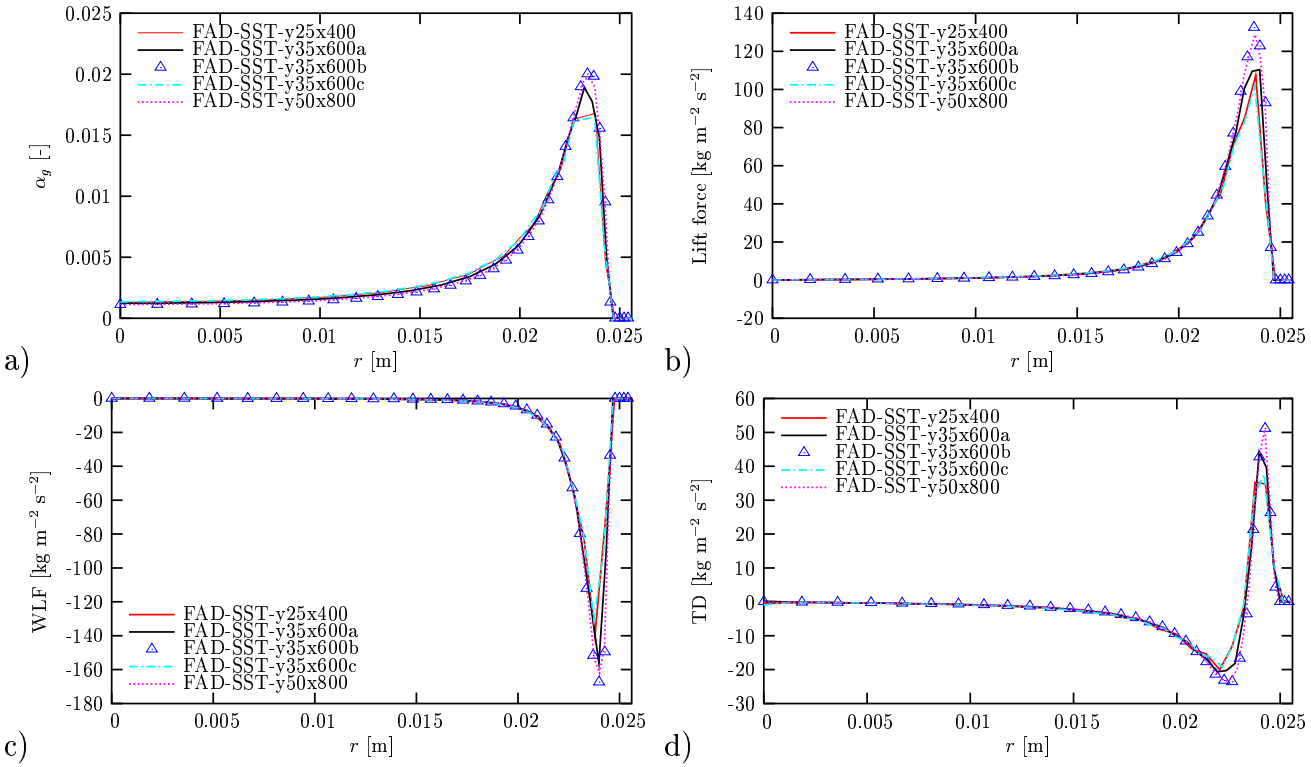

Figure 2: FZR-042: numerical results ($L/D = 59.2$) based on different grids: gas volume fraction (a), lift force (b), wall lubrication force (c), and turbulence dispersion force (d).

normalized air volume fraction, which is defined by eq. (13), were compared at the cross section chosen for validation, $L/D = 59.2$.

$$\alpha_g^* = \frac{\alpha_g}{\alpha_{g,0}}, \text{ with } \alpha_{g,0} = 2\int_0^1 \alpha_g(r^*)\, r^* \mathrm{d}r^* \tag{13}$$

As shown in Fig. 3 (left), all inlet profiles lead to the same gas volume fraction distribution at $L/D = 59.2$. Hence it is advantageous to make model validation at this cross section. In addition, the sensitivity of the results to the bubble diameter was examined. In contrast to the negligible effect of the inlet condition, the bubble diameter was found to have a strong influence on the gas volume fraction profile (Fig. 3, right). This result is consistent with experimental

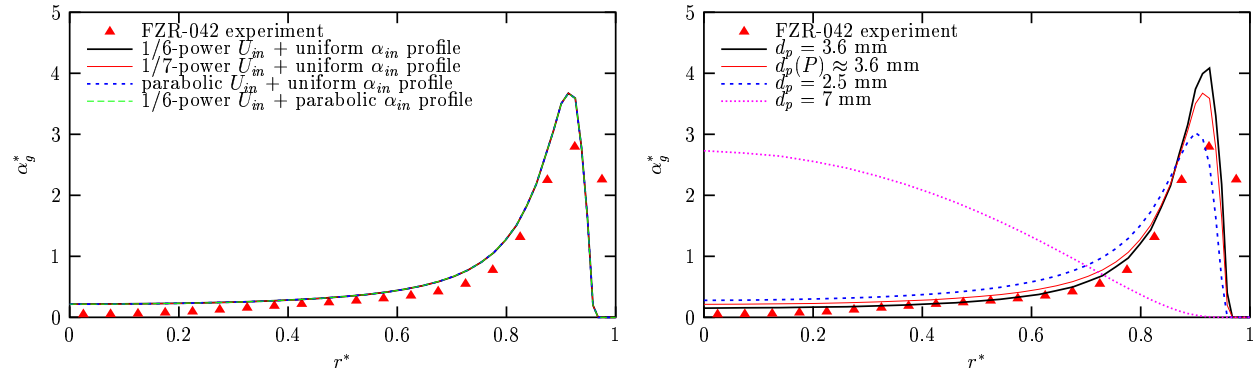

Figure 3: Comparison of the gas volume fraction distribution at $L/D = 59.2$ under various inlet conditions (left) and for different mean bubble diameters (right).

observations (Liu, 1993; Prasser et al., 2001) and is due to the fact that the interfacial forces are functions of the bubble diameter. Refer to Table 1, the measured mean diameter is 3.6 mm in the case FZR-042. The notation $d_p(P)$ means considering the dependence of bubble diameter on the local pressure in estimation of the interfacial forces but keeping the incompressible fluid assumption. The other diameter values were simply assumed for control. It can be seen in Fig. 3 (right), a central gas peak occured for $d_p = 7$ mm due to the negative lift coefficient. The sensitive dependency of the gas volume fraction on the bubble diameter also suggest the need to develope poly-disperse models to consider the bubble size effect more accurately.

5.3 Evaluation and discussion

It was noticed during the investigation that the turbulence model has a strong effect on the gas volume fraction distribution. Therefore, we performed case study for FZR-074 and FZR-042 by applying the SST and k-ε model to the liquid phase turbulence in combination with the FAD or RPI model for the turbulent dispersion force. A turbulence coeficient, $C_{TD} = 0.35$, was chosen for the RPI model. The results are displayed in Fig. 4. It can be observed that the SST-FAD combination produced relatively good agreements with the corresponding measurements in both cases. The k-ε model predicted an unrealistcally high gas peak close to the wall and a too low gas concentration in the core region compared to the measurements. It was interesting to note that the numerical results based on the two turbulence models became close to each other if the gas volume fraction at the inlet was reduced to a negligible value. These results suggest that a further work on multiphase flow turbulence modeling is very necessary in order to understand the remarkable difference in the numerical results caused by the turbulence model. Here we simply chose SST model for its superior performance. In addition, it is observed from Fig. 4 that the gas volume fraction obtained using the RPI model is lower in the core region than those based on the FAD model in both cases. This indicates a stronger turbulence dispersion force given by the latter. The difference of the results is not essential in case FZR-042. Nevertheless, the FAD model led to much better agreements with the experimental data in the case FZR-074 though the core gas concentration was still underpredicted. This deviation can be reduced by using two fluids for the gas phase, namely separating the larger bubbles (negative lift force) from the small ones in future investigation considering the strong influence of the bubble diameter. Further results on the turbulent dispersion force model effect will be presented later.

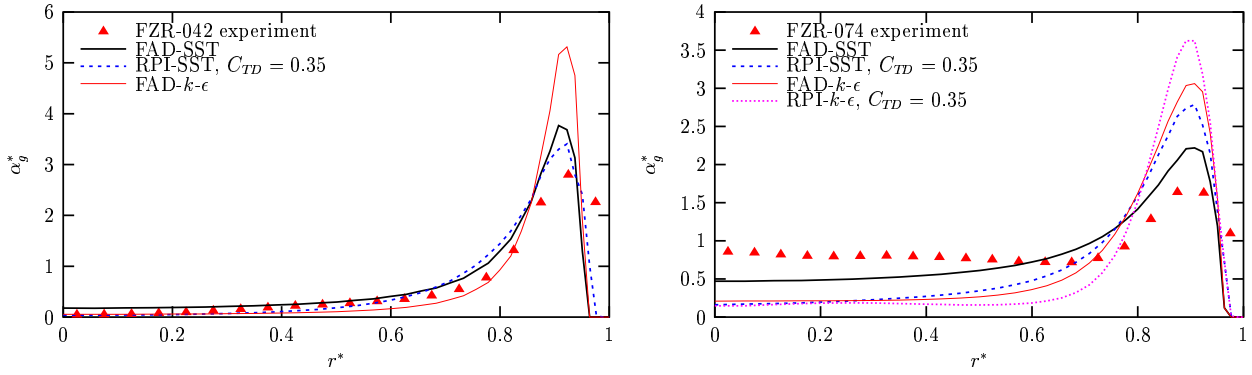

Figure 4: Case study: compare the turbulence and turbulent dispersion force model.

Comparisons were also made for the CFX-5.6 standard wall lubrication force model (6) proposed by Antal et al. (1991) and the Tomiyama formulation (7). As demonstrated in Fig. 5, the wall lubrication force given by the Antal's model is obviously too weak to balance the Tomiyama lift force (4). For this reason, this combination caused a strong overprediction of

the gas volume fraction in the wall proximity (Fig. 5, left) and even caused oscillation in the numerical solution when the two grids with the finest near wall resolution were applied (Fig. 5, right). This problem was not overcomed by using other model coefficients, e.g., those applied

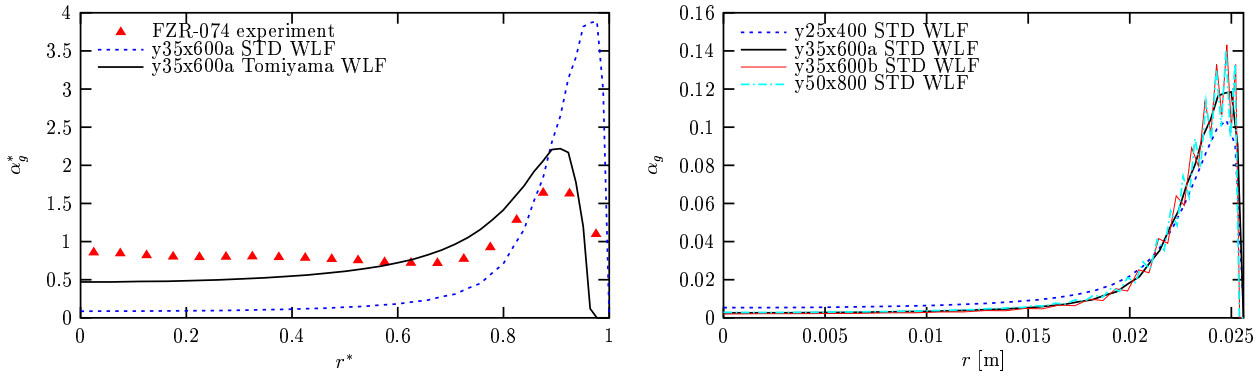

Figure 5: FZR-074: compare the wall lubrication force models: Tomiyama WLF (7) vs. the CFX-5.6 standard (STD) WLF (6).

by Krepper and Prasser (2000) as discussed in section 3.2. Although the present results do not allow us to conclude that the Tomiyama model (7) is overall superior to the Antal model (6), the disadvantage of the latter in application and the weakness in its derivation are obvious. Therefore, the Tomiyama formulation (7) was adopted in the present investigation.

In summary, the Tomiyama lift (4) and wall lubrication force model (7) and the SST model were applied in the simulations of further test cases based on the above case studies. Calculations were performed using the RPI and FAD model for the turbulent dispersion force. The numerical results for the gas volume fraction profile at $L/D = 59.2$ are displayed in Fig. 7

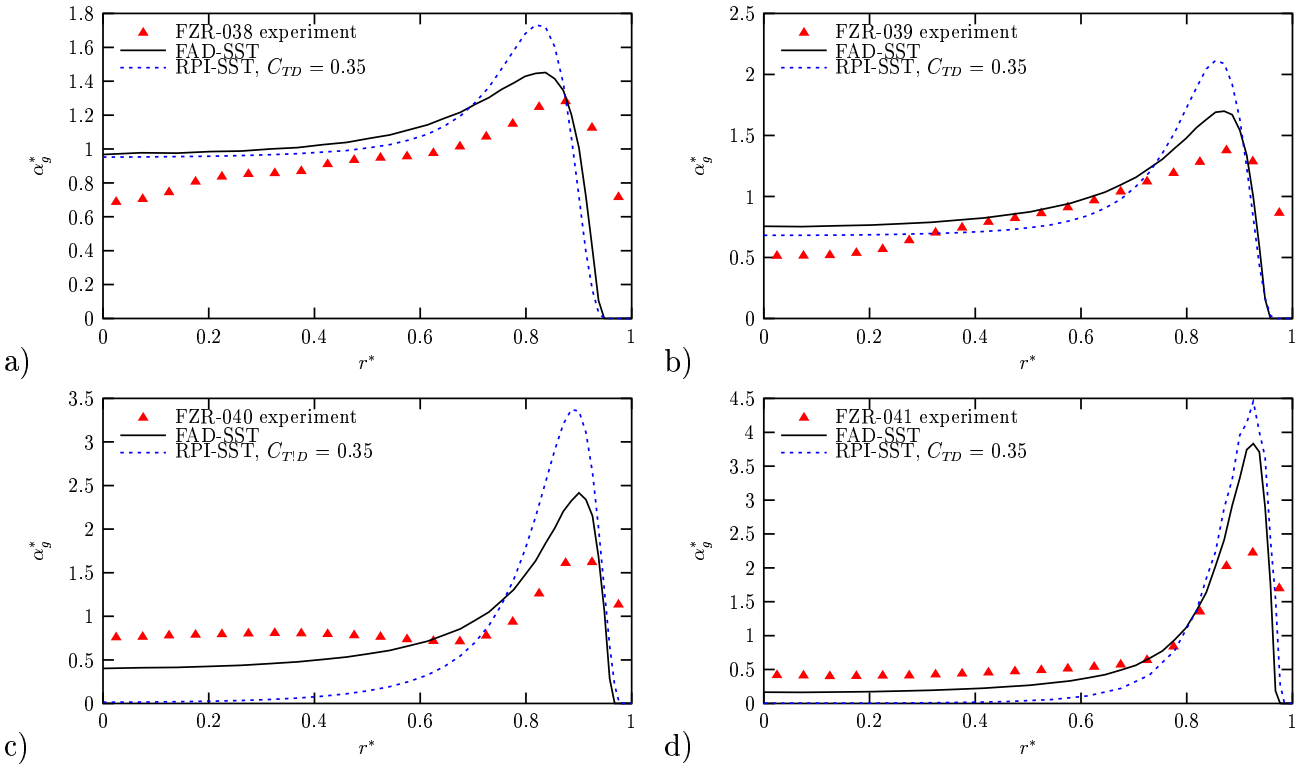

Figure 6: Further comparisons between the FAD and RPI model.

together with the corresponding measurement data. It can be observed that all numerical results based on the FAD model agree fairly well with the experimental data. Similar to the observation to FZR-074 and FZR-042 (Fig. 4), the RPI model overpredicted the wall gas peak and in the same time underpredicted the core gas concentration in all cases. In order to make a direct comparision for both models, the corresponding turbulent dispersion force coefficient of the FAD model was estimated for all test cases using eq. (11) and is plotted in Fig. 7 together with a constant coefficient $C_{TD} = 0.35$ used in the RPI model. The results clearly show that the turbulent dispersion force given by the RPI model is much too weak except for in the near-wall region. Moreover, Fig. 7 also showes that a constant coefficient C_{TD} as assumed in the RPI model is not realistic. Due to this oversimplification, the RPI model does not take into account a number of physical dependencies appearing in eq. (11). In addition, it is interesting to note that C_{TD} decreases with increasing superficial velocity of the continuous phase (refer to Table 1). This behavior might be easier to understand by referring to the discussions provided in section 3.3. The bubble response time τ_d is similar for all test cases due to their similar d_p, whereas τ_e decreases with increasing flow Reynold numbers. That explains the above observation.

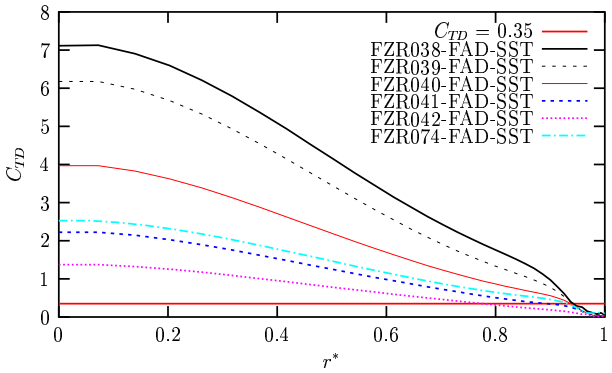

Figure 7: Equivalent turbulent dispersion force coefficient (11) of FAD model in analogy to the RPI model.

Despite the acceptable agreements between numerical results and measurements achieved using the above non-drag force models, it is necessary to address the limitation of the present study. Firstly, the bubble coalescence and breakup was neglected in the investigation. Larger bubbles which receive a negative lift force were also not distinguished from small bubbles. This might be the main reason responsible for the deviations observed in the core region. In addition, the numerical results indicate a bubble free region in the wall proximity, which is different from the experimental data. A number of causes can have contributed to this deviation, e.g., the decreased measurement accuracy in the wall proximity and the inaccuracy of the wall lubrication force models. Refering to Fig. 5, a bubble free region did not occur when the Antal's wall lubrication force model (6) was applied. Hence these results suggest that the Tomiyama model (7) might produce a too strong wall lubrication force.

6 Summary and conclusion

In this work, a number of non-drag force models were implemented in the Eulerian multiphase flow package of the commercial code CFX-5.6. Extensive validation and model evaluation were carried out based on the experimental data for upwards air-water bubbly flow in a vertical pipe measured at the FZR MT-Loop facility. The numerical results of the local gas volume fraction

distribution were compared with the corresponding experimental data measured at the cross section located at $L/D = 59.2$ from the gas injection. Fairly good agreements were obtained by using the Tomiyama's model of lift and wall lubrication force and the FAD model for the turbulent dispersion force in combiniation with the SST model for the continuous phase turbulence. The investigation clearly showes that the FAD model for the turbulent dispersion force is superior to the RPI model widely applied in literature. The results also suggest that further efforts in improving multiphase turbulence models, near-wall closures and in developing polydisperse multi-fluid models including the coalescence and breakup process are very necessary.

7 Acknowledgment

The present work was a result of close collaboration between FZR and ANSYS Germany in the framework of the GRS-BMWA network projects. The model implementation and validation were made by Th. Frank and J.-M. Shi. The experimental studies were performed by the other coauthers at FZR. The financial support from Ministry of Economy and Labor (BMWA) of Germany to the FZR authors in the project "TOPFLOW - transient two phase flow test facility for generic investigation of two phase flows and further development and validation of CFD codes" and to ANSYS Germany GmbH in the CFD network project "Development of CFD codes for multidimentional flows in reactor safety applications" are gratefully acknowledged.

References

Antal, S., Lahey, R., Flaherty, J., 1991. Analysis of phase distribution in fully developed lminar bubbly two-phase flow. Int. J. Multiphase Flow 7, 635–652.

Auton, T., 1987. The lift force on a spherical body in a rotational flow. J. Fluid Mech. 183, 199–218.

Burns, A., 2001. Turbulence dispersion forces in multiphase flow. Tech. rep., AEA Technology plc.

Burns, A., Frank, T., Hamill, I., Shi, J.-M., 2004. The Favré averaged drag model for turbulence dispersion in Eulerian multiphase flow. In: 5th International Conference on Multiphase Flow, ICMF'04, May 30-June 4,2004.

Drew, D., 2001. A turbulence dispersion model for particles or bubbles. J Eng. Math. 41, 259–274.

Drew, D., Passman, S., 1999. Theory of Multicomponent Fluids. Springer.

Frank, T., 2002. Parallele Algorithmen für die numerische Simulation dreidimensionaler, disperser Mehrphasenströmungen und deren Anwendung in der Verfahrenstechnik. Berichte aus der Strömungstechnik. Shaker Verlag.

Frank, T., 2003. A review on advanced Eulerian multiphase flow modeling for gas-liquid flow. Tech. Rep. TR-03-08, ANSYS CFX Germany.

Frank, T., Shi, J.-M., Burns, A., 2004. Validation of Eulerian multiphase flow models for nuclear safety safety applications. In: 3rd International Symposium on Two-Phase Flow Modelling and Experimentation,22-24 September 2004. Pisa, Italy, pp. 1–8.

Gosman, A., Issa, T., Likakou, C., Looney, M., Politis, S., 1992. Multidimensional modeling of turbulent two-phase flows in stirred vessels. AIChE J 38, 1946–1956.

Ishii, M., 1975. Thermo-Fluid Dynamic Theory of Two-Phase Flow, Eyrolles Book Pulbication. Eyrolles Book Pulbication.

Krepper, E., Prasser, H.-M., 2000. Measurements and CFX simulations of a bubbly flow in a vertical pipe. In: AMIFESF Workshop, Computing methods for two-phase flow. pp. 1–8.

Kurose, R., Misumi, R., Komori, S., 2001. Drag and lift forces acting on a spherical bubble in a linear shear flow. Int. J. Multiphase Flow 27, 1247–1258.

Legendre, D., Magnaudet, J., 1998. The lift force on a spherical bubble in a viscous linear shear flow. J Fluid Mech 368, 81–126.

Liu, T., 1993. Bubble size and entrance length on void development. Int J Multiphase Flow 19, 99–113.

Lopez de Bertodano, A., 1998. Two fluid model for two-phase turbulent jets. Nuclear Engng. Design 179, 65–74.

Lopez de Bertodano, A., Lahey, R., Jones, O., 1994. Development of a $k - \epsilon$ model for bubbly two-phase flow. Trans. ASME J. Fluids Eng. 116, 128.

Lucas, D., Krepper, E., Prasser, H.-M., 2002. Experimental high-resolution database for co-current air-water flow in a vertical pipe. In: 40th European Two-Phase Flow Group meeting, Stockholm, Sweden, June 10-13, 2002. p. Paper C4.

Lucas, D., Krepper, E., Prasser, H.-M., 2003. Evolution of flow patterns, gas fraction profiles and bubble size distributions in gas-liquid flows in vertical tubes. Transactions of the Institute of Fluid-Flow Machinery 112, 37–46.

Magnaudet, J., Eames, I., 2000. The motion of high-Reynolds-number bubbles in inhomogeneous flows. Annu. Rev. Fluid Mech. 32, 659–708.

Mei, R., 1992. An approximate expression for the shear lift force on a spherical particle at finite reynolds number. Int. J. Multiphase Flow 18, 145–147.

Mei, R., Clausner, J., 1994. Shear lift force on a spherical bubble. Int. J. Heat and Fluid Flow 15, 62–65.

Menter, F., 1994. Two-equation eddy-viscosity turbulence models for engineering applictions. AIAA-Journal 32.

Moraga, F., Bonetto, F., Lahey, R., 1999. Latteral forces on spheres in turbulent uniform shear flow. Int. J. Multiphase Flow 25, 1321–1372.

Moraga, F., Larreteguy, A., Drew, D., Lahey, R., 2003. Assesment of turbulence dispersion models for bubbly flows in the low stokes number limit. Int. J. Multiphase Flow 29, 655–673.

Prasser, H.-M., Böttger, A., Zschau, J., 1998. A new electrode-mesh tomograph for gas-liquid flows. Flow Measurement and Instrumentation.

Prasser, H.-M., Krepper, E., Lucas, D., 2002. Evolution of the two-phase flow in a vertical tube - decomposition of gas fraction profiles according to bubble size classes using wire-mesh sensors. Int. J. of Thermal Sciences 41, 17–28.

Prasser, H.-M., Lucas, D., Krepper, E., Baldauf, D., Böttger, A., Rohde, U., et al., 2003. Strömungskarten und Modelle für transiente zweiphasenströmungen. Tech. Rep. FZR-379, Forschungszentrum Rossendorf.

Prasser, H.-M., Scholz, D., Zippe, C., 2001. Bubble size measurement using wire-mesh sensors. Flow Measurement and Instrumentation 12, 299–312.

Saffman, P., 1965a. Corrigendum to "The lift on a small sphere in a slow shear flow, JFM 22:385-400, 1965". J. Fluid Mech. 31, 624.

Saffman, P., 1965b. The lift on a small sphere in a slow shear flow. J. Fluid Mech. 22, 385–400.

Sato, Y., Sadatomi, M., Sekoguchi, K., 1981. Momentum and heat transfer in two-phase bubbly flow. Int J Multiphase Flow 7, 167–178.

Simonin, O., 2000. Statistical and continuum modelling of turbulent reactive particulate flow. In: Buchlin, J.-M. (Ed.), Theoretical and Experimental Modeling of Particulate Flow. VKI Lecture Series 2000-06. von Karman Institute for Fluid Dynamics.

Tomiyama, A., 1998. Struggle with computational bubble dynamics. In: Third International Conference on Multiphase Flow, ICMF 98. Lyon, France.

Tomiyama, A., Sou, A., Zun, I., Kanami, N., Sakaguchi, T., 1995. Effect of Eötvös number and dimensionless liquid volumetric flux on lateral montion of a bubble in a liminar duct flow. In: Serizawa, A., Fukano, T., Bataille, J. (Eds.), Advances in Multiphase Flow. Elsevier Science, pp. 3–15.

Tomiyama, A., Zun, I., Tamai, H., Hosokawa, S., Okuda, T., 1999. Measurements of traverse migration of single bubbles in a couette flow. In: Two-Phase Flow Modelling and Experimentation. Edizioni ETS Italy, pp. 941–948.